View Article Online
View Journal

Biomaterials Science

Accepted Manuscript

This article can be cited before page numbers have been issued, to do this please use: P. T. M. Phuong, H. Jhon, I. In and S. Y. Park, *Biomater. Sci.*, 2019, DOI: 10.1039/C9BM00734B.

ROYAL SOCIETY OF CHEMISTRY

rsc.li/biomaterials-science

View Article Online
DOI: 10.1039/C9BM00734B

Journal Name

ARTICLE

Photothermal Modulated Reversible Volume Transition of Wireless Hydrogel Embedded with Redox-responsive Carbon Dot

Received 00th January 20xx,
Accepted 00th January 20xx

DOI: 10.1039/x0xx00000x

www.rsc.org/

Pham Thi My Phuong[a], Heesauk Jhon[b], Insik In[a,c], Sung Young Park[a,d*]

The reversible volume transition of redox-responsive hydrogels by near-infrared (NIR) irradiation has recently attracted significant attention as a novel therapy matrix for tracking and treating cancer via stimuli-responsive fluorescent on/off with controllable volume transition with wireless sensing system. A NIR-induced redox-sensitive hydrogel was synthesized by blending with IR825-loaded carbon dot (CD) for enhanced mobility of the nanoparticles inside gel network achieving reversible volume phase transition remotely controlled by a smartphone application via inducing different redox environments. The presence of CD-IR825 in the thermosensitive poly(N-isopropylacrylamide) hydrogel network imparted fluorescent, electronic and photothermal properties to the hydrogels, which resulted in volume shrinking behavior upon exposure to NIR laser irradiation due to the redox-sensitive CD. Under the NIR on/off cycles, the photothermal temperature, fluorescence, and porous structure were reversed back after turning off the NIR laser. The hydrogel responsiveness under GSH and NIR light via wireless device was studied via the changes of resistance graph on a smartphone application, generating a fast and simple method for observing hydrogel properties. The *in vitro* cell viabilities of MDAMB cancer cells incubated with the composite hydrogel in the presence of external GSH exhibited a higher photothermal temperature, and the cancer cells were effectively killed after NIR irradiation. Therefore, the NIR-induced redox-responsive nanocomposite hydrogel prepared herein has potential in cancer treatment and will allow for the study of nanoparticle motion in hydrogel networks under multiple stimuli via a wireless device with a faster and more convenient method.

Introduction

Numerous studies regarding nanocomposite hydrogels obtained from the incorporation of inorganic, metallic, polymeric, and carbon-based nanomaterials into matrices have been reported. The addition of these particles can reinforce the hydrogel and impart external stimuli responsiveness to thermal, magnetic, electric, and mechanical stimuli. Hence, as hydrogel-based sensors, these hybrid systems can be used to control the release profile of drugs or other molecules from the hydrogel system to specific surrounding environments.[1–4] As a host matrix for the immobilization of guest biomolecules, physical changes in the hydrogel can be exploited as a sensing method using various externally-added molecules that affect the structural and mechanical behaviors of the blended hydrogel system.

Hydrogels can exhibit volume or phase transitions in response to external stimuli such as pH,[5–7] temperature,[8,9] ionic concentration,[10,11] solvent composition,[12–14] and light intensity.[15,16] These "smart" hydrogels have been applied in fields such as biomedicine, pharmacy, biotechnology, bioengineering, and agriculture. Recently, reduction sensitive hydrogels have been fabricated using disulfide cross-linkers.[17,18] The disulfide bond can be cleaved by various reducing agents, such as dithiothreitol (DTT),[19] tributylphosphine (TBP),[20] tris(2-carboxyethyl) phosphine (TCEP),[21] and glutathione (GSH)[22] due to thiol-disulfide exchange reactions.[23–25] Glutathione is the most abundant non-protein thiol in eukaryotic cells with an intracellular concentration in cancer cells significantly higher (~ 4-fold) than that of normal cells (2–5 mM).[26] By incorporating multiple-responsive nanoparticles into the hydrogel network, the microstructure can be controlled via rheological and volumetric changes to trigger drug/molecule release under the appropriate physiological conditions.[27,28]

By combining imaging agents and/or therapeutic molecules, near-infrared (NIR)-responsive carbon dot (CD) can be used in potential therapies for tracking and treating cancer. Previous studies have attached/loaded NIR agents into fluorescent CD systems to overcome NIR fluorescent dyes drawbacks.[29–32] Recent studies have focused on electrochemical changes for the responsiveness of hybrid hydrogel under various stimuli such as redox, light, etc. that showed higher sensitivity and simplicity with the innovation by connecting to wireless smartphone as a portable device for real-time monitoring sensor.[33–35] By combining with wireless sensing device, the study of responsiveness under different stimuli was simplified with high

[a.] Department of IT Convergence, Korea National University of Transportation, Chungju 380-702, Republic of Korea
[b.] Department of Electronics, Information and Communication Engineering, Mokpo National University, Muan-gun 58554, Republic of Korea
[c.] Department of Polymer Science and Engineering, Korea National University of Transportation, Chungju 380-702, Republic of Korea
[d.] Department of Chemical and Biological Engineering, Korea National University of Transportation, Chungju 380-702, Republic of Korea
Tel: +82-43-841-5221, Email: parkchem@ut.ac.kr (Sung Young Park)
*Corresponding authors
Electronic Supplementary Information (ESI) available: DOI: 10.1039/x0xx00000x

View Article Online
DOI: 10.1039/C9BM00734B

sensitivity, accuracy by inexpensive and flexible wireless platform. In this study, a thermosensitive PNIPAM hydrogel was blended with NIR-redox-sensitive fluorescent CD (CD-IR825) nanoparticles to study the effect of NIR light and GSH on the controllable thermo-sensitivity of the hydrogel based on the photothermal temperature. The composite hydrogel was expected to own fluorescent, redox, and photothermal properties arising from the CD-IR825, which might be quenched upon thermal changes. Moreover, the electronic properties of the composite hydrogel depending on GSH and NIR stimuli was also investigated by connecting with a wireless system including Bluetooth module for data transmission via changes of resistance signal represented on the smartphone. This study of the nanocomposite hydrogel could offer a novel insight into nanoparticle mobility and behavior in hydrogels via wireless device detection, which is important for the further development and characterization of future stimuli-responsive hydrogels.

Experimental Section

Materials and Characterization

N-Isopropylacrylamide (NIPAM), methylene bis-acrylamide (MBA), ammonium persulfate (APS), N,N,N',N'-tetramethyl-ethylenediamine (TEMED), branched polyethyleneimine (bPEI, Mw: 2,000), 3,3-dithio-bis-(sulfosuccinimidyl) propionate (DSP), H_2SO_4, dimethylformamide (DMF), phosphate buffered saline (PBS) solution, and glutathione (GSH) were obtained from Sigma-Aldrich (USA). Propidium iodide (PI) and calcein-AM were purchased from Molecular Probe, Life Technologies (Invitrogen). Penicillin-streptomycin, fetal bovine serum (FBS), trypsin-EDTA (ethylenediaminetetraacetic acid) solution, and Roswell Park Memorial Institute (RPMI)-1640 medium were obtained from Gibco BRL, USA. The MDAMB-231 human cell line was obtained from the Korean Cell Line Bank (Seoul, Korea). The heptamethine indocyanine dye IR825 was synthesized using a previously described method.[32]

Proton nuclear magnetic resonance (^{1}H-NMR) spectra were recorded using a 400-MHz Bruker Advance spectrometer with d_6-DMSO as a solvent. UV-visible spectra were obtained using a 2020 Optizen UV spectrophotometer (Mecasys Co., Korea). The particle size was measured by dynamic light scattering (DLS) using a Zetasizer Nano (Malvern, Germany) instrument. The fluorescent properties of the hydrogels were investigated using an EVOS FL fluorescence microscope (Life technologies, USA) and PL spectra were recorded using a L550B luminescence spectrometer (Perkin Elmer). The X-ray photoelectron spectroscopy (XPS) results were obtained using an Omicrometer ESCALAB (Omicrometer, Taunusstein, Germany) instrument. Confocal images were captured on a LSM510 confocal laser scanning microscope (Carl Zeiss, Germany). Photothermal therapy (PTT) effects were measured using an infrared camera (NEC Avio, Thermo Tracer TH9100) and an 808 nm NIR laser (PSU-III-LRD, CNI Optoelectronics Tech. Co. LTD, China). Field-emission scanning electron microscopy (FE-SEM) micrographs were obtained using a SEM/EDX instrument (JSM-6700F, JEOL, Musashino, Akishima, Tokyo, Japan). The rheological properties of the incorporated hydrogels were evaluated using a rheometer (AR 1500EX, TA Instruments Korea, USA) with a 20 mm parallel plate on a Peltier plate in frequency sweep mode at a 1.0% strain amplitude (linear region) with angular frequency ranging from 0.1 to 100 rad/s. The electrochemical property was confirmed using an electrochemical impedance spectrometer (CS350, CorrTest Instrument, China). The hydrogel behavior under GSH and NIR treatments was studied via wireless device consisting of Arduino Uno microcontroller (ATmega328P Processor) as a sensing part and smartphone as real-time data output that connected via bluetooth module (AppGosu) as wireless communicator.

Synthesis of carbon dot (CD)

First, bPEI (1.0 mmol) in DMF was mixed with 3,3-dithio-bis-(sulfosuccinimidyl) propionate (DSP) (0.5 mmol) in a dropwise manner and reacted for 2 h. Subsequently, PBS (pH 7.4) was used to stop reaction for 15 min at room temperature. Afterwards, the solution was dialyzed (molecular weight cut-off (MWCO): 3.5 kDa) for 3 days and freeze-dried to obtain disulfide crosslinked bPEI (PEI-S-S-PEI). Fluorescent CD was then prepared via acid-catalyzed carbonization. In detail, 1 g of PEI-S-S-PEI was dissolved in 5 mL of double-distilled water (DDW) and 10 mL of concentrated H_2SO_4 solution was then added with 1 min stirring and 3 min shaking. Afterwards, the solution was diluted with 185 mL DDW and dialyzed for 1 day (MWCO: 1 kDa) and the CD was collected by freeze-drying.[36]

Synthesis of the IR825 loaded CD (CD-IR825)

Briefly, 100 mg of the CD was loaded with different amounts of IR825: 1, 5, and 25 mg (referred to as CD-IR825 (0.01), CD-IR825 (0.05), and CD-IR825 (0.25), respectively) by physical mixing with PBS 7.4 as solvent at room temperature for 24 h. This was followed by dialysis to remove the non-reactants for 1 day (MWCO: 1 kDa). After 24 h, the product inside the membrane was collected and freeze-dried.

Synthesis of the CD-IR825-embedded hydrogel

Three types of hydrogels (Hydrogel 1, Hydrogel 2 and Hydrogel 3) were prepared as follows: 283 mg NIPAM, 12.5 mg MBA crosslinker, and 3 mg of CD-IR825 (0.01) for Hydrogel 1, CD-IR825 (0.05) for Hydrogel 2, and CD-IR825 (0.25) for Hydrogel 3 were dissolved in 5 mL DDW. Subsequently, 10 mg APS and 10 µL TEMED were added to the solution and mixed well, then casted into a well plate before solidification. After that, the synthesized hydrogels were freeze dried for further use. A PNIPAM hydrogel without CD-IR825 (Hydrogel 0) was used as a control.

Temperature-sensitivity of the composite hydrogels

The composite hydrogels were incubated in GSH solution (0 or 10 mM) for 24 h, then removed and observed under a fluorescence microscope and photoluminescence (PL) spectrometer at 25 and 37 °C.

View Article Online
DOI: 10.1039/C9BM00734B

NIR light-responsive properties

To investigate the temperature and structural changes of the hydrogels in response to NIR light, the swollen hydrogel discs at similar swelling ratios (~1600%) were incubated in GSH solutions (0 or 10 mM) at 37 °C for 24 h, then removed and the isolated gels were irradiated with NIR light at power density of 2 W/cm^2 at room condition. The temperature elevation of the hydrogel was recorded over 20 min of irradiation.

NIR-dependent swelling ratio (SR) based on the redox environment

The NIR-dependent swelling capacity depending on redox condition was measured at room temperature by initially immersing the weighed (W_0) lyophilized cylindrical samples in 0.1 M PBS 7.4 (0 and 10 mM GSH). The swollen hydrogels were removed after 1 h, immediately weighed (W_t) after removing excess water, irradiated with/without NIR laser for 2 min and continued swelling in those solutions. Afterwards, the swelling ratios were measured at specific times over the next 40 h.

Reversibility of the composite hydrogels: photothermal, fluorescent, mechanical, and swelling ratios

To investigate the NIR light-responsive reversibility of the nanocomposite hydrogels via NIR on/off, the non-GSH and GSH-treated hydrogel discs were exposed to NIR light (2 W/cm^2) at room temperature for 4 cycles of 2 min laser-on and 5 min laser-off. The temperature elevation, fluorescence, mechanical/structural properties, and swelling ratios of the hydrogel discs during each on/off cycle was examined using a digital camera, PL spectrophotometer, SEM, rheometer, and analytical balance. Additional experiments were performed by spraying a small amount of DDW at the cooling point, waiting for 5 min, then initiating the next NIR on/off cycle to observe the effect of dehydration on recovering of photothermal, fluorescence, mechanical properties, pore size, and swelling ratios.

Electroconductivity property of Hydrogel

Herein, Hydrogel 3 was chosen to investigate the electronic properties under GSH and NIR light stimuli by connecting to the system including working, reference, and counter electrodes *via* copper wires. The fitting-curved resistance was analyzed using electrochemical impedance spectroscopy (EIS) of CS350 Potentiostat Electrochemical Station, Corrtest. China.

Redox- and NIR- responsive photothermal properties of Hydrogel via wireless device

The volume phase transition and electronic properties of redox-sensitive hydrogel can be observed by connecting with wireless device that resulted *via* AppGosu application in smartphone. In details, the 0 mM and 10 mM treated hydrogel 3 were first connected to Arduino Uno microcontroller system *via* copper wire electrodes. The changes of resistance graph after GSH treatment and 2-min NIR irradiation were achieved by wireless access between smartphone and Arduino Uno microcontroller using Bluetooth module (AppGosu). The system was showed in **Figure S7** (Supporting Information)**.**

Cell viability experiment

The MDAMB cells were grown in RPMI medium supplemented with FBS, 0.25% w/v penicillin, and 0.05% w/v trypsin. The cells were then detached from the culture surface via trypsinization, collected by centrifugation, and dispersed in new media. The photothermal properties and cell viability after incubation with hydrogel and NIR irradiation was observed via a live/dead assay. Briefly, 1 mL of MDAMB cells solution at 1 × 10^5 cells/mL were added to each well of a 6-well plate to incubate with the hydrogels for 5 min at 37 °C under a 5% humidified CO_2 atmosphere and with/without the external addition of 10 mM GSH. Afterwards, the treated hydrogels in the cell solution were subsequently illuminated with an 808 nm laser at a power density of 2 W/cm^2 for 2 min. Finally, the cells were stained with calcein-AM and PI, then observed and quantified using a confocal laser scanning microscope to image the stained (live/dead) cells. The increase in the temperature of the hydrogel discs was examined using a digital camera.

View Article Online
DOI: 10.1039/C9BM00734B

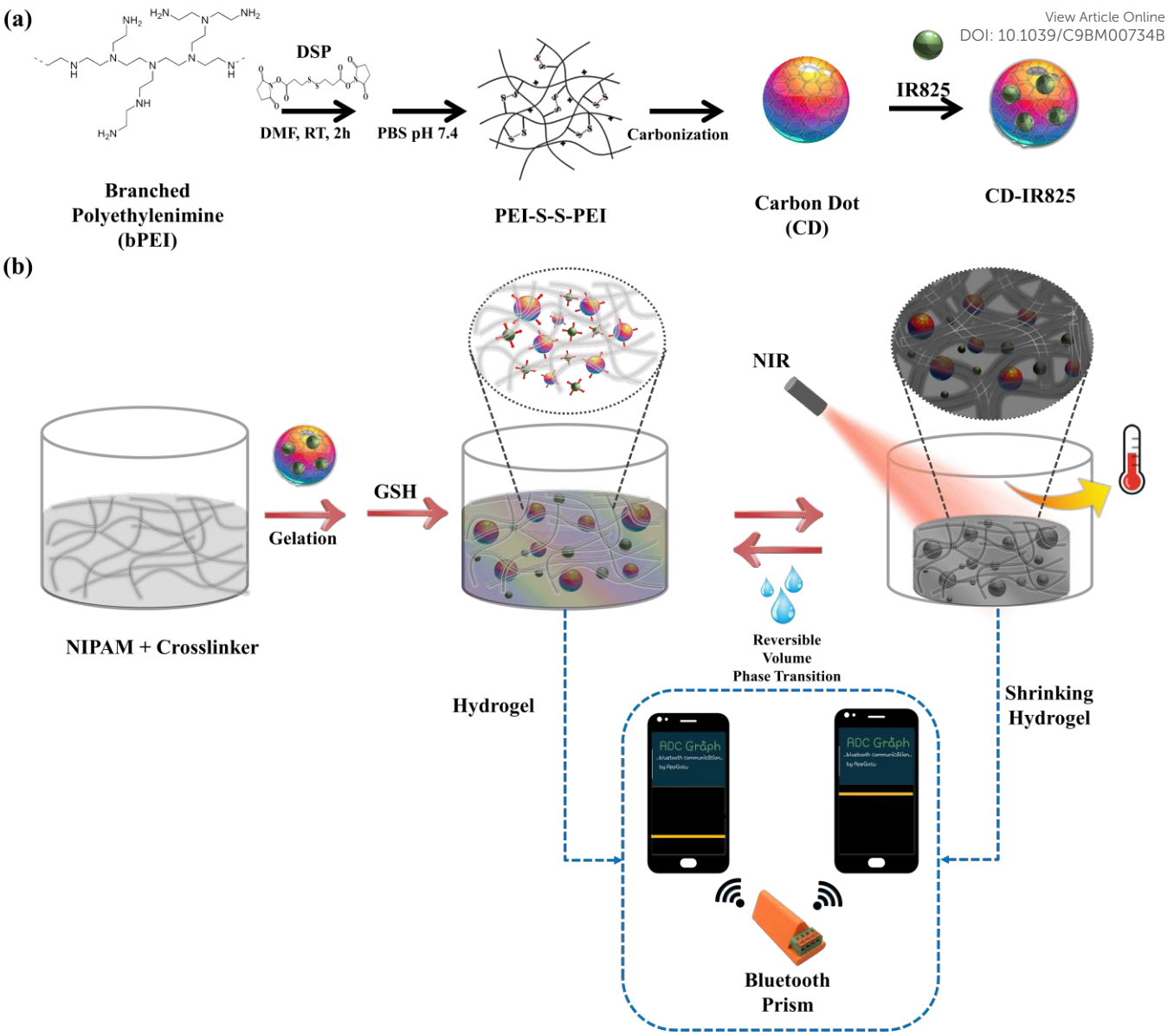

Scheme 1. Scheme illustrating (a) the synthesis of IR825-loaded CD (CD-IR825) and (b) the NIR mediated redox-responsive CD embedded in the hydrogel for reversible volume phase transition detected via wireless device.

Result and Discussion

The NIR-induced redox-responsive CD-embedded wireless hydrogel was obtained by physically mixing the IR825-loaded CD (CD-IR825) into the thermo-sensitive PNIPAM hydrogel network. The cationic redox-responsive CD was obtained from carbonized disulfide crosslinked bPEI, followed by loading different amounts of NIR dye via hydrophobic interaction for the photothermal effect (CD-IR825). The incorporation of CD-IR825 into the PNIPAM hydrogel network contributed to the redox response of the composite hydrogel after GSH treatment that resulted in fluorescence, PTT effect and electronic responses upon NIR irradiation. Under NIR exposure, the composite hydrogels shrunk, which quenched the fluorescence and hindered nanoparticle mobility. The photothermal heat affected the physical and structural properties of the composite hydrogel which were reversible with the addition of water after cooling. The electronic properties of the hydrogels under stimulation of GSH and NIR light were performed by real-time resistance graph via connection between the wireless module of Arduino microcontroller and smartphone as data receiver that generated a significant increase of resistance value at shrinking state. Further investigation of the NIR-induced killing effect of the composite hydrogel towards MBAMB cancer cells showed highly effective anticancer ability under NIR irradiation with the addition of external GSH. Hence, this study offers novel insight into nanoparticle mobility and behavior in hydrogels, which is important for the further development of stimuli-responsive hydrogels (**Scheme 1**).

View Article Online
DOI: 10.1039/C9BM00734B

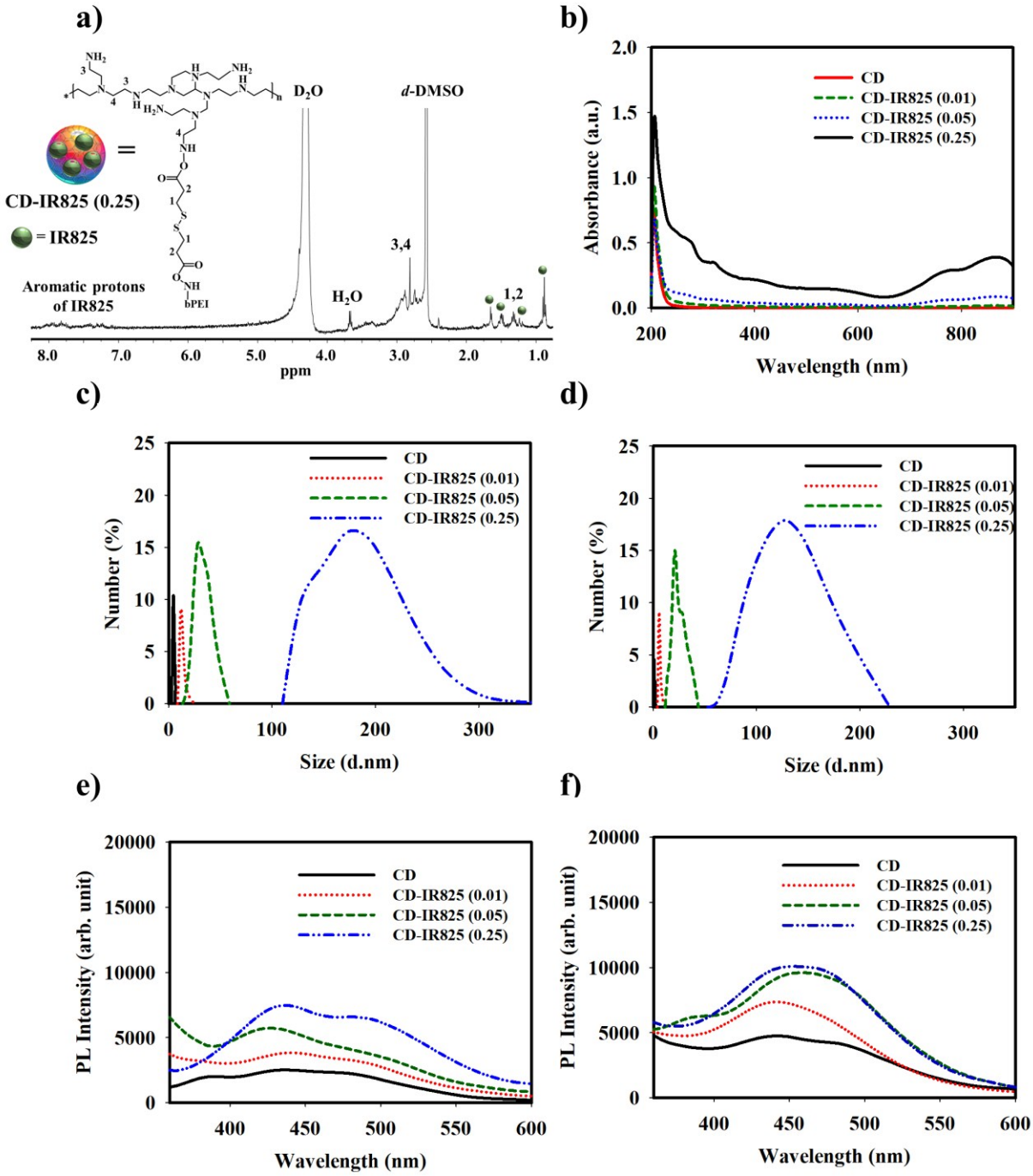

Figure 1. (a) ^{1}H-NMR spectra of the CD-IR825 (0.25) nanoparticles in co-solvents of D_2O: *d*-DMSO (3:7, v/v ratio); (b) UV-vis before and after loading different amounts of IR825; DLS and PL spectra after incubation with (c, e) 0 mM GSH and (d, f) 10 mM GSH (Concentration: 0.1 mg/mL).

View Article Online
DOI: 10.1039/C9BM00734B

Characterization of the IR825 dye loaded redox-responsive CD nanoparticles (CD-IR825)

First, CD was synthesized via acid-catalyzed carbonization of the disulfide-crosslinked branched polyethyleneimine (PEI-S-S-PEI) polymer. The chemical structure of the IR825-loaded CD (CD-IR825) before and after loading the photothermal dye-IR825 was confirmed by ^{1}H NMR and UV-vis spectroscopy. As shown in **Figure 1a**, the peaks at 7.2–8.3 ppm arise from the aromatic protons of IR825, confirming that IR825 was successfully loaded into the CD cores.[37] The higher loading amount of IR825, higher intense peaks of methylene protons of IR825 were also detected at 0.8–1.96 ppm (**Figure S1**).[38,39] As different amounts of IR825 were loaded, peaks in the 600 to 1000 nm range in the UV-vis spectrum were observed with the increasing absorbance intensity, confirming the successful incorporation of IR825 into the CDs (**Figure 1b**). [29,40,41] The hydrophobicity of the crosslinked sites on the CD core caused IR825 to assemble at those sites via hydrophobic interactions upon simple physical mixing for 24 h. The hydrodynamic size of the CD increased with increasing amount of loaded IR825, as shown in **Figure 1c**. **Figure 1d** shows the effect of GSH on the CD-IR825 nanoparticles, which included crosslinked site breakage, resulting in a reduction of particle size after 24 h of incubation. After loading IR825, the PL spectra shifted to an emission of 500 nm and the fluorescent intensities were enhanced with increasing amounts of IR825 (**Figure 1e**).[42,43] Because of the aggregation in aqueous state, the graphitized cores of CD and IR825 will suffer π–π stacking hydrophobic interactions, resulting in enhanced red-shifted emission due to aggregation-induced emission (AIE).[44,45] After treatment with 10 mM GSH, the fluorescent intensities increased due to the increased surface area caused by disulfide cleavages, as shown in **Figure 1f**.[46]

View Article Online
DOI: 10.1039/C9BM00734B

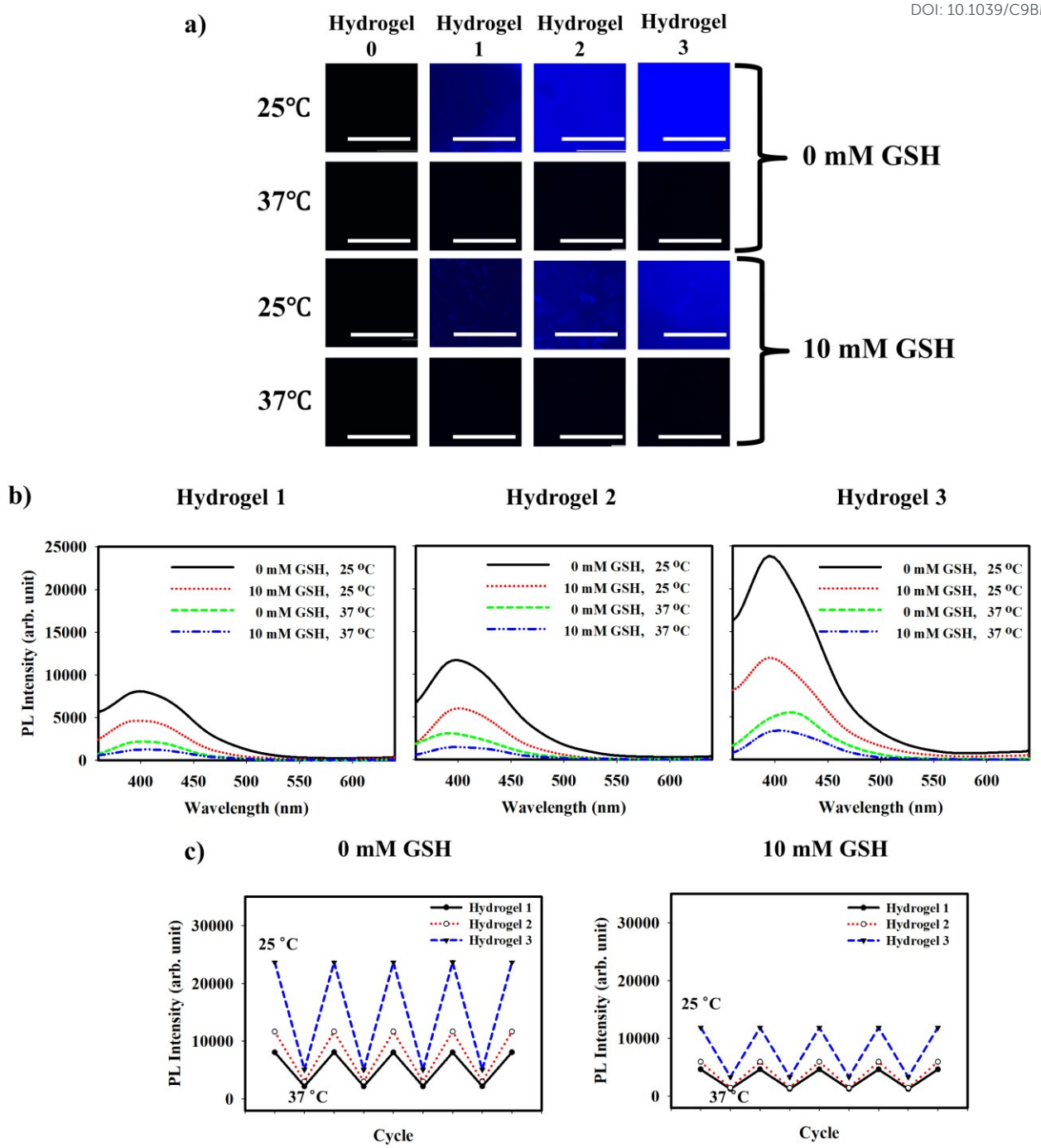

Figure 2. Thermosensitivity of the composite hydrogels. (a) Fluorescent microscopy (scale bar: 1000 μm), (b) PL spectra, and (c) Reversible PL depending on temperature (25 and 37 °C) and redox conditions (0 and 10 mM of GSH).

Characterization of the temperature reversible CD-IR825 embedded in PNIPAM hydrogels

The NIR-induced temperature reversible hydrogels (Hydrogel 0, Hydrogel 1, Hydrogel 2 and Hydrogel 3) were formed by physically mixing different CD-IR825 nanoparticles and the crosslinked PNIPAM (no CD-IR825, CD-IR825 (0.01), CD-IR825 (0.05) and CD-IR825 (0.25), respectively) during hydrogel preparation. This was performed to study the reversible memory storage of the composite hydrogels based on temperature changes with fluorescent on/off behavior. After hydrogel formation, XPS was used to determine the compositions of the composite hydrogels (**Figure S2**). The narrow-scanned spectrum of C 1s of the hydrogels exhibited peaks at 286.5 and 283.4 eV, arising from C-Cl and C=C of the IR825 and CD structure. These peaks were not observed in the spectrum of the pure PNIPAM hydrogel, indicating the successful incorporation of CD-

View Article Online
DOI: 10.1039/C9BM00734D

IR825.[47,48] It is likely that after incorporation of CD-IR825 into the PNIPAM hydrogel network, the composite hydrogel exhibited fluorescence and photothermal properties arising from the imbedded CD-IR825, which could heat the hydrogel under NIR irradiation and quench fluorescence with rising temperature.[49,50] As shown in **Figure 2a**, the composite hydrogels showed stronger fluorescent signals with increasing content of IR825 due to stronger AIE effect (**Figure 1e**). For all samples, at room temperature the CD-IR825 nanoparticles were dispersed in the transparent hydrogel matrix and exhibited strong fluorescent emission. After incubation in a 10 mM GSH solution, the fluorescent intensities of the composite hydrogels decreased due to the partial release of free CD (4% of Hydrogel 1, 5% of Hydrogel 2, and 7% of Hydrogel 3) into the incubation solutions after cleavage of the disulfide linkages (**Figure 2b**). However, the composite hydrogels treated with 0 and 10 mM of GSH exhibited shrinking behavior with a significant reduction in fluorescent signal after 5 min incubation at 37 °C due to the lower critical solution temperature (LCST) nature of the PNIPAM hydrogel.[51] The collapsed PNIPAM particles likely acted as a strong scattering center to quench the fluorescence signal of CD-IR825, resulting in the dramatic decrease in the fluorescence intensity. Thus, the fluorescence of the hydrogels was suppressed considerably at high temperatures by the hydrophobic interaction of PNIPAM.[52] Furthermore, the effect of temperature on the fluorescent properties of the composite hydrogels was observed via fluorescence spectra of the composite hydrogels measured during a temperature change between room temperature (25 °C) and physiological temperature (37 °C). It is clear that the fluorescence intensity of the hydrogels decreased abruptly with increasing temperature and the composite hydrogels maintained excellent reversible thermo-induced swelling/shrinking behavior between 25 and 37 °C, as shown in **Figure 2c**.[53]

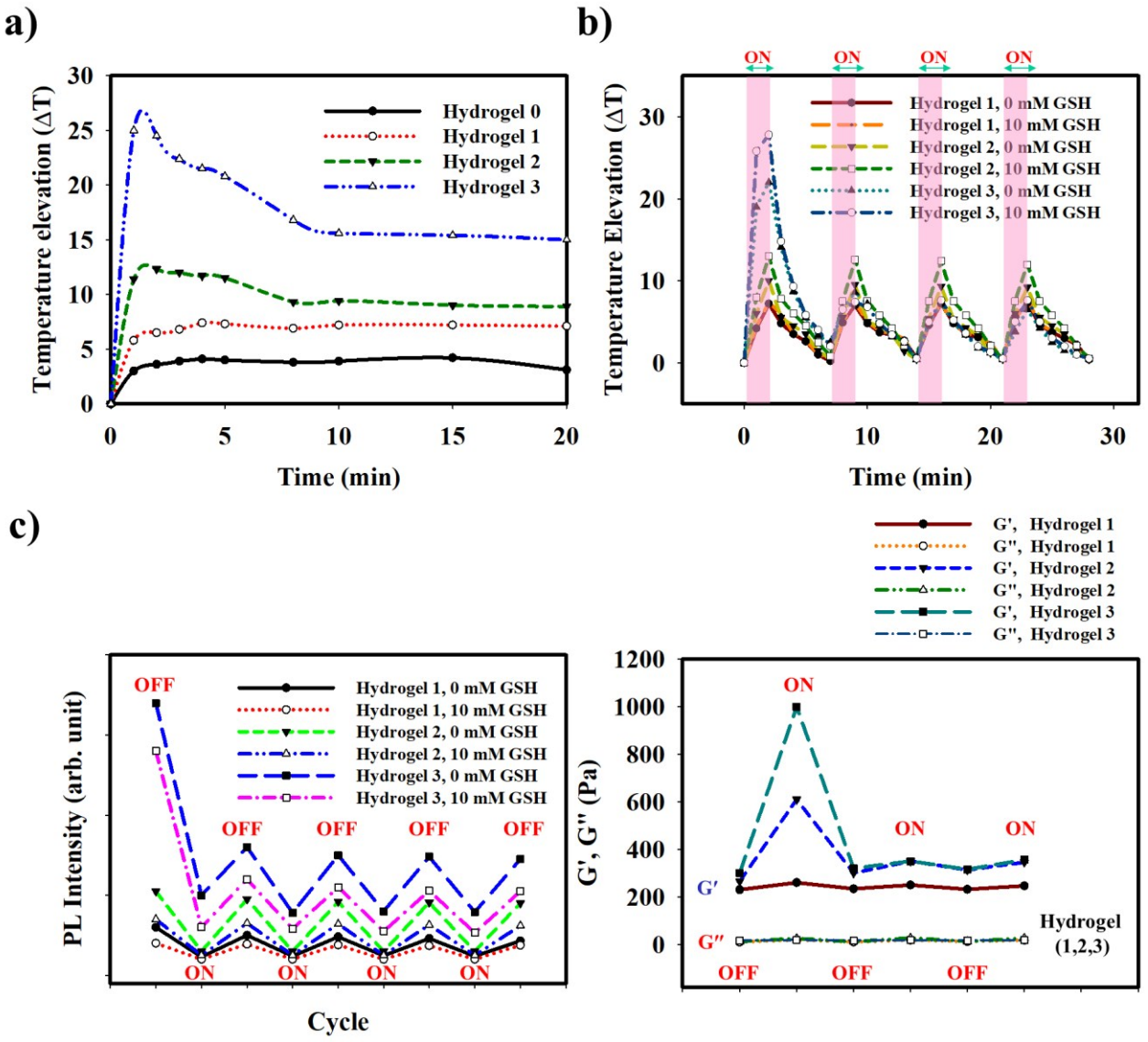

View Article Online
DOI: 10.1039/C9BM00734B

Figure 3. (a) Photothermal temperature elevation curve obtained during 20 min NIR irradiation and the NIR on/off/on cycles-based reversibility of (b) PTT, (c) PL and (d) modulus changes of Hydrogel 1, Hydrogel 2, and Hydrogel 3 under 10 mM GSH treatment.

NIR-responsive properties of hydrogel

IR825 exhibited excellent photothermal effects, so the composite hydrogel was examined for its photothermal effects upon irradiation after incorporation of CD-IR825.[54] First, all kinds of CD-IR825 nanoparticles rapidly converted NIR light into thermal energy as highly localized heat sources when irradiated with an 808 nm laser for 2 min and plateaued until 5 min of irradiation (**Figure S3**). Higher amounts of IR825 loaded into the CD showed higher PTT effects with elevated temperatures after GSH treatment. Afterwards, the CD-IR825 nanoparticles were blended inside of the PNIPAM hydrogel network. As illustrated in **Figure 3a**, the temperature of Hydrogel 3 increased much faster than that of Hydrogel 1 due to the enhanced photothermal effect of the CD-IR825 (0.25) nanoparticles compared to that of the other samples. The temperature of Hydrogel 0 did not significantly increase as it did not contain the photothermal CD-IR825. After irradiation for 1.5 min, the gel started shrinking immediately after exposed to NIR irradiation, and the temperature of Hydrogel 3 increased approximately 27 °C after GSH treatment, compared to a 20 °C change without GSH due to the enhanced IR825 mobility after cleaving the disulfide bonds of CD-IR825 (**Figure S4a**). With continued irradiation for 20 min, the temperature of Hydrogel 3 began to decrease after 3 min and remained at ΔT ~ 12 °C. This can be explained by dehydration and shrinking volume of the hydrogel that limited the mobility of IR825 inside the hydrogel network upon irradiation.[55]

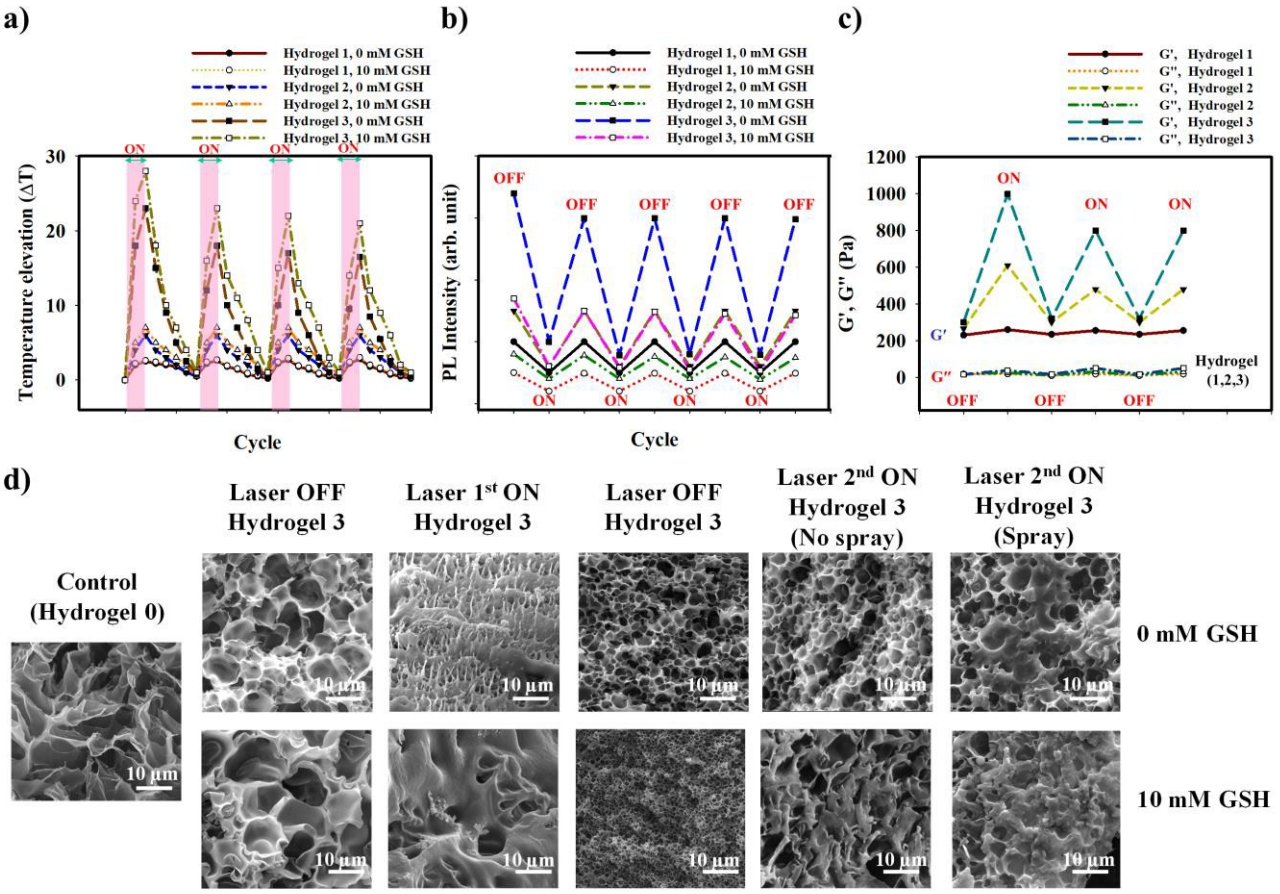

Figure 4. Reversibility of the composite hydrogel after spraying: (a) PTT and (b) PL, (c) modulus changes and (d) SEM images of Hydrogel 3 after 10 mM GSH treatment and after on-off-on NIR; pure PNIPAM (Hydrogel 0) was used as a control.

View Article Online
DOI: 10.1039/C9BM00734B

Reversibility of the NIR-responsive properties of the hydrogel

Next, the reversibility of the composite hydrogel under on/off NIR laser based on elevated temperature, fluorescence, swelling ratio, surface topography, and mechanical properties was studied. As shown in **Figure 3b**, all composite hydrogels could efficiently convert the NIR adsorption into heat during the first on cycle within 2 min to reach ΔT ~ 27 °C after the 10 mM GSH treatment, as observed by the shrinking behavior of the hydrogels. The hydrogels were cooled for 5 min and irradiated again for the next NIR on cycle. However, the photothermal effect in the second cycle significantly decreased, indicating that the mobility of the nanoparticles inside the matrix was interrupted due to shrinking caused by dehydration after the first cycle of NIR illumination. Simultaneously, the fluorescent intensities of the hydrogels were examined, and the same patterns were observed (**Figure 3c)**. The experiment was also performed with the addition of a small amount of water after the first NIR irradiation cycle. Interestingly, the photothermal effect and fluorescent signals recovered to ~ 80% in the second and subsequent cycles (**Figure 4a and 4b,** respectively). This indicated that the mobility of the embedded nanoparticles was mostly recovered inside the hydrogel system after providing rehydrating water.[56] As shown in **Figure S5**, the hydrogel absorbed the supplied water with the recovered swelling degrees after spraying, which resulted in the recovery of the original photothermal effect and fluorescence signal.

The thermo-sensitivity of the composite hydrogels was characterized based on storage (G') and loss moduli (G") during the on-off-on NIR irradiation. As a result, the value of G' was much higher than that of the loss modulus G", indicating suggesting the excellent elasticity of the composite hydrogels. After irradiation, G' increased significantly due to the high temperature and a lower storage modulus was observed after 10 mM GSH treatment (**Figure 3d)** compared to GSH untreated samples (**Figure S4b)**.[57] The increased storage modulus was caused by the increasing IR825 concentration that absorbed more light. After cooling, the modulus reverted to its original state and could hardly return to the highest modulus values. Nevertheless, the modulus was regained after spraying during the second cycle of NIR irradiation, confirming the effect of adding water in enhancing nanoparticle mobility inside the hydrogel network in both treated (**Figure 4c)** and GSH untreated (**Figure S4c)** GSH samples. These results indicated that the composite hydrogel can absorb NIR energy to produce heat with a higher amount of photothermal agents and that the NIR-responsiveness properties can be controlled by water addition.

Moreover, the microstructural changes in the composite hydrogels in response to NIR irradiation were investigated. The swollen and shrunk samples of hydrogel 3 after on-off-on NIR cycles were processed by freeze-drying and characterized by high-magnification SEM. **Figure 4d** shows the cross-sections of Hydrogel 3 (after 0 and 10 mM GSH treatment) before and after exposure to the on/off NIR laser without spraying. Before irradiation, Hydrogel 3 exhibited an interconnected microporous structure with an increased pore size compared to the microporous structure of pure PNIPAM (Hydrogel 0) due to the repulsion of amine groups in the CD.[58] After the first cycle of NIR irradiation, the internal microporous structure collapsed by aggregation due to shrinking of composite hydrogel induced by the photothermal heat.[59] The GSH-treated hydrogel adopted a more condensed structure, showing larger volume contraction caused by the enhanced heat generation after breaking the disulfide linkages between CD and IR825. After the NIR laser was turned off for 5 min, the hydrogel shrank its microporous structure significantly compared to the untreated gel, while the pore size of the 10 mM GSH-treated samples was much smaller than that of the GSH-untreated sample. In the second ON cycle of NIR irradiation, the hydrogel was not able to return to its original state, and insufficient heat was available to aggregate, similar to the first cycle. However, upon addition of water after the first irradiation, the collapsed state was almost recovered, corresponding to the previous photothermal results. Therefore, the microstructure behavior of the hydrogel is related to the volume change of the PNIPAM hydrogel under NIR irradiation. After irradiation, the NIR-sensitive nanoparticles CD-IR825 absorbed light and converted it into heat, which was more dominant than the PNIPAM's LCST behavior that caused dehydration, resulting in water loss in the matrix that inhibited nanoparticle motion inside the hydrogel matrix.

Swelling ratio of the hydrogel dependent on NIR and redox responsiveness

As shown in **Figure 5a**, the swelling ratios of the composite hydrogel after incorporation CD:IR825 nanoparticles was largely unchanged without GSH treatment. However, when treated with the GSH solution, the swelling ratios of all composite hydrogels remarkably increased, compared to Hydrogel 0 (**Figure 5b)**. The microstructure of the treated hydrogels was observed by SEM, showing the largest increase in the pore size in Hydrogel 3 after GSH treatment (**Figure S6)**. This is due to the cleavage of disulfide bonds of CD-IR825 based on branched PEI which subsequently generated free CD and IR825 nanoparticles inside the network, resulting in the increase of CD mobility that could enhance the water adsorption due to highly hydrophilic nature of branched PEI.[58,60,61] After 1 h of reswelling in PBS solutions (0 or 10 mM GSH), the composite hydrogels were subjected to 2 min of NIR irradiation and continued swelling until reaching the maximum swelling ratio after 40 h. Interestingly, the equilibrium swelling ratios significantly decreased in all samples after exposure to NIR irradiation, where the composite hydrogels treated with GSH showed decreased swelling ratios compared to those of the samples treated with GSH-free solution, as shown in **Figure 5c** and **5d**. [62] In addition, the NIR-irradiated hydrogels showed more condensed structure after GSH treatment and swelling for 24 h after irradiation compared to those of the untreated specimens, in agreement with the swelling ratio results shown in **Figure S6.**

View Article Online
DOI: 10.1039/C9BM00734B

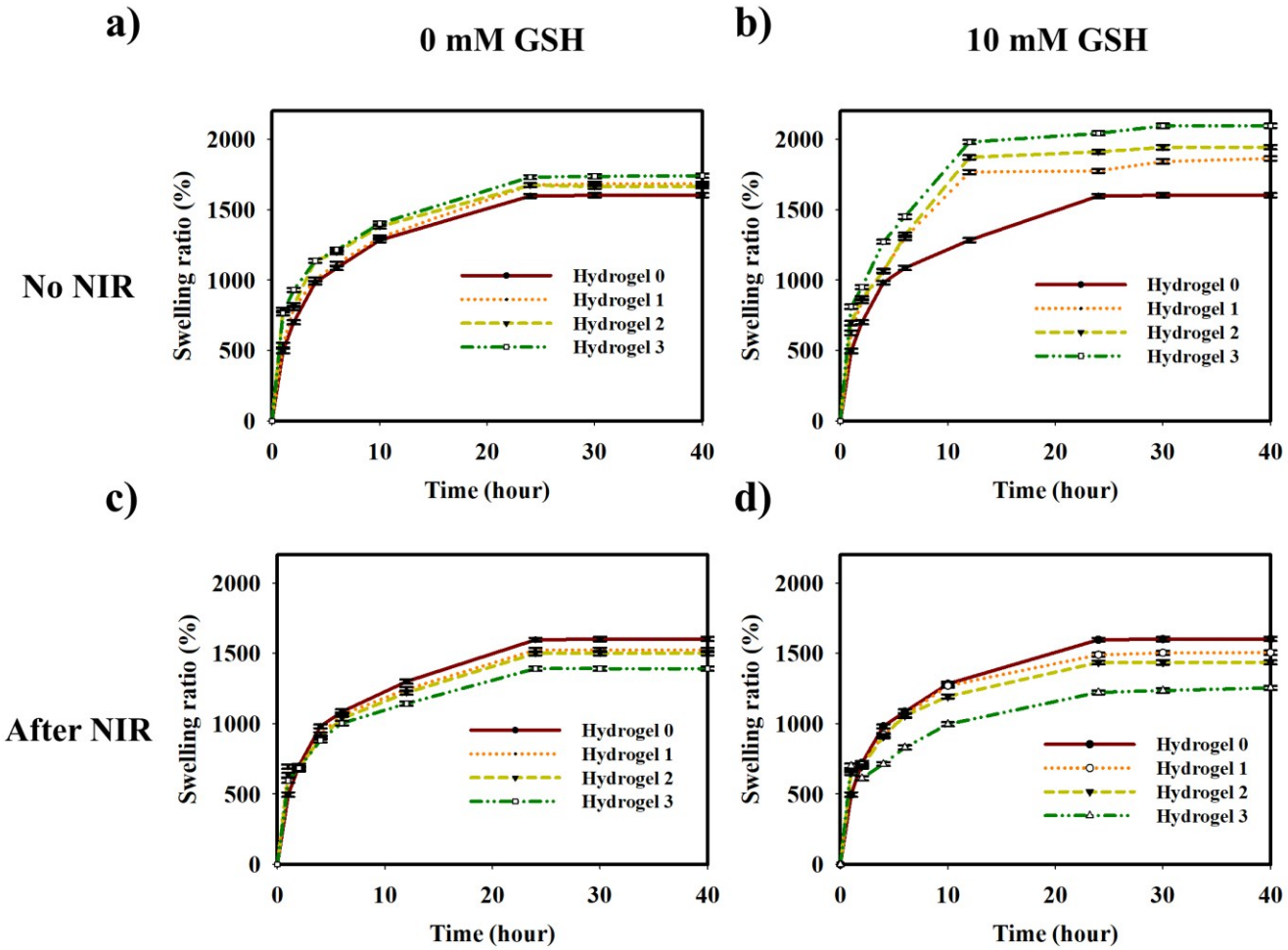

Figure 5. Time-dependent swelling ratios of composite hydrogels in (a, b) before and (c, d) after 2 min of NIR irradiation in (a, c) 0 mM GSH and (b, d) 10 mM GSH solutions.

Electronic properties depending on GSH and NIR light stimuli studies via wireless device

To achieve the responsiveness of the composite hydrogel under different stimuli agents, we next conducted the electronic performance for Hydrogel 3 under different redox conditions and NIR illumination by EIS measurement. As shown in **Figure 6a**, the Hydrogel 3 initially showed the charge transfer resistance (R_{ct}) at 2878 Ω, then notably increased to 7076 Ω after 10 mM GSH treatment. The lower electrical performance after breakdown of disulfide linkages by GSH treatment implied the random disperse of the separated smaller nanoparticles of sp^2-riched carbon dot in the hydrogel network, compared to continuous path for transporting electron of the CD-IR825 nanoparticles in the composite hydrogel after *in situ* formation.[63,64] The R_{ct} of the Hydrogel 3 to the electrode surface was performed after irradiating by NIR laser for 2 min, resulting in noteworthy enhancement of resistance at 10910 Ω that reflected the higher contraction behavior of the composite hydrogel after GSH treatment. By underwent NIR irradiation for 2 min, Hydrogel 3 shrank due to water loss in the hydrogel matrix and the decrease of contacting area between Hydrogel 3 and the electrodes, subsequently affecting the conductivity properties of the composite hydrogel.[65,66] Furthermore, we observed the redox and NIR light-responsive properties of the hydrogel in terms of electrical signal via real-time measurement by wireless device. By connecting the composite hydrogel with the wireless system including Arduino Uno microcontroller and Bluetooth module via copper wires (as shown in **Figure S7**), the signals were expressed as resistance graph that can be easily observed by smartphone application (AppGoSu), consistently with the EIS data by the significant rise of resistance after NIR irradiation (**Figure 6b**). The resistance line on the application moved up, representing the enhancement of resistance of the system with the biggest gap after irradiated by NIR laser of GSH-treated sample.

View Article Online
DOI: 10.1039/C9BM00734B

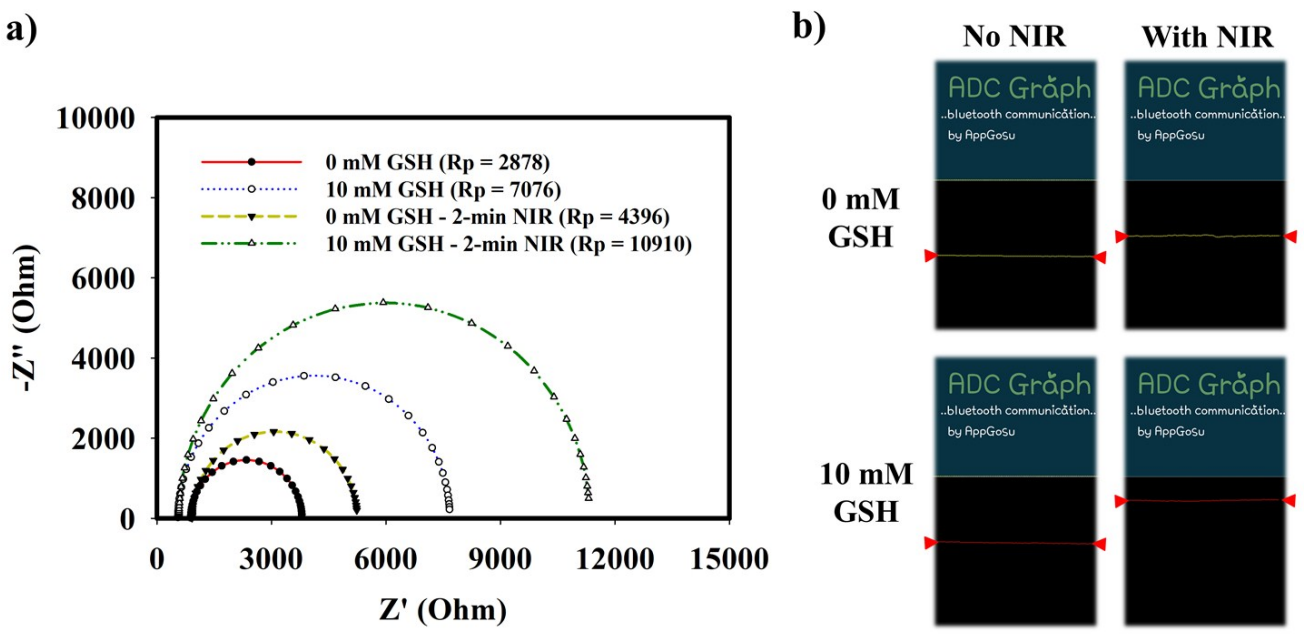

Figure 6. (a) The electrochemical impedance spectroscopy (EIS) analysis and (b) corresponding resistance output screenshotted from smartphone using wireless device (Airduno) of the Hydrogel 3 after incubation with 0 mM and 10 mM GSH and exposed to NIR laser (808 nm, 2 W/cm^2) for 2 min.

***In vitro* cytotoxicity assay based on the photothermal effect of the hydrogel**

The localized photothermal effects of the nanocomposite hydrogel on the MDAMB cells were assessed following exposure to the NIR laser for 2 min.[67,68] As shown in **Figure 7a**, cells incubated with pure PNIPAM hydrogel disks showed no significant temperature difference between the cells with or without GSH addition during laser irradiation. With increasing IR825 content, the photothermal effect was enhanced and the gel supplemented with GSH achieved higher temperatures. Subsequently, the cellular viability was determined after the cancer cells were incubated with the prepared hydrogels for 5 min after the 2 min laser irradiation. Composite hydrogel 3 was heated to ~ 42 °C (ΔT ~ 18°C) after incubation with an additional 10 mM GSH in the cell solution, which much higher than the sample in GSH-free media. More than 95% of the cells were viable when treated with the PNIPAM hydrogel, but with increasing IR825 content of the composite hydrogels, the MDAMB cell viabilities dramatically decreased from 90% for Hydrogel 1 to 85% and 21% for Hydrogel 2 and Hydrogel 3, respectively. Similarly, lower cell viabilities were observed in cells treated with hydrogels treated with GSH (85%, 76%, and 10%, for Hydrogels 1, 2, and 3, respectively, **Figure 7b**). In addition, to determine the cell viabilities before and after NIR irradiation as well as GSH responsiveness, the live and dead assay was performed, which involves fluorescence labeling with calcein-AM (green) for live cells and propidium iodide (red) for dead cells (**Figure 7c**). The high photothermal heat produced during NIR exposure effectively killed more than 90% of cancer cells treated with hydrogel 3 after GSH supplementation. These results demonstrated that the nanocomposite hydrogels can rapidly and efficiently convert NIR light into thermal energy as highly localized heat sources to directly kill cancer cells, showing great potential for thermal cancer therapy.

View Article Online
DOI: 10.1039/C9BM00734B

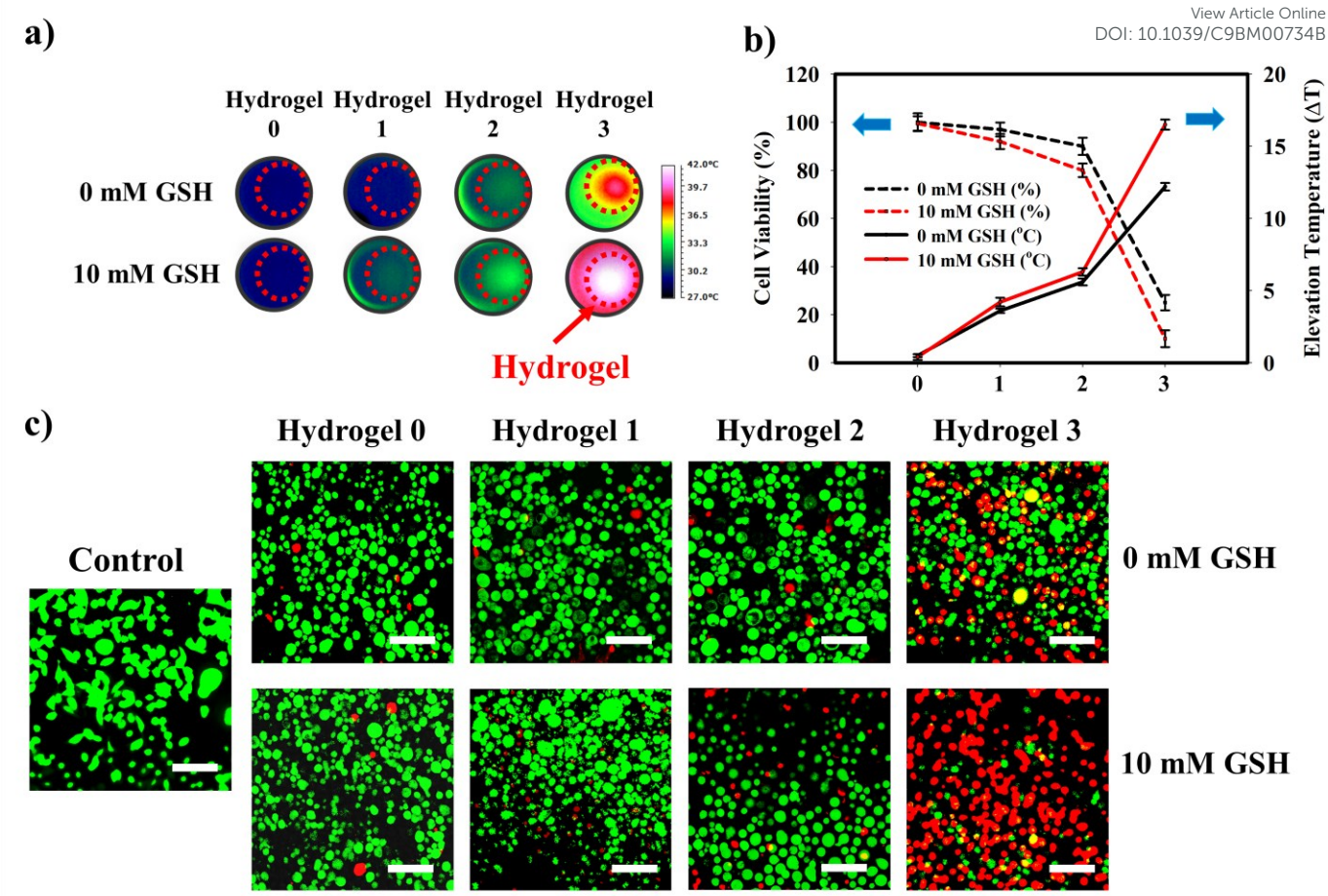

Figure 7. *In vitro* cytotoxicity of the nanocomposite hydrogels with the addition of 0 and 10 mM GSH. (a) Infrared thermal images after incubation of the hydrogel with the cells and exposure to NIR laser irradiation (808 nm, 2 W/cm^2) for 2 min. (b) Cell viability and corresponding temperature changes and (c) live/dead assay of each composite hydrogel incubated with MDAMB cells after NIR laser irradiation. Scale bar: 100 µm.

Conclusions

In conclusion, dual NIR-induced redox-sensitive hydrogels for reversible volume phase transition were successfully synthesized with unique fluorescent, thermosensitive, electronic and photothermal properties after incorporations of IR825-loaded carbon dot (CD-IR825). The embedding of CD-IR825 to the PNIPAM hydrogel network by physical mixing caused the composite hydrogels to exhibit fluorescent and photothermal properties, which could be quenched under NIR irradiation. The redox responsiveness of the composite hydrogels was confirmed by the enhanced photothermal temperature after GSH treatment, further easily confirmed via wireless device. The heat converted from the absorbed NIR light affected the fluorescent, physical, and structural properties of the composite hydrogels, exhibiting shrinking behavior after irradiation. The reversibility of the composite hydrogels with NIR on/off cycles was demonstrated, indicating that the photothermal heat, fluorescence, and structure of the prepared hydrogels was reversible by water addition after turning off the NIR laser. The changes of electronic properties of the composite hydrogel under stimulations of GSH and NIR light were studied via EIS and wireless-based system via smartphone that showed a fast and efficient pathway to study hydrogel properties under stimuli. Further observation of the killing efficiency of MDAMB cancer cells *in vitro* confirmed that the composite hydrogels generated a higher photothermal temperature with external GSH addition, effectively killing more than 80% of cells after NIR irradiation. This also confirmed the higher mobility of the nanoparticles inside gel network in a tumor environment. Therefore, the developed light- and redox-sensitive nanocomposite hydrogels have great potential in the study of the effect of nanoparticles motion in hydrogel networks with dual triggers for wireless sensing ability and can be applied for improvement of cancer therapies in the future.

Conflicts of interest

The authors declare that they have no competing financial interests.

View Article Online
DOI: 10.1039/C9BM00734B

Acknowledgements

This research was supported by Grant No. P00008500 from the Ministry of Trade, Industry & Energy (MOTIE) and the Basic Science Research Program through the National Research Foundation of Korea (NRF) funded by the Ministry of Education (NRF-2017R1A2B2002365 and 2018R1A6A1A03023788).

1 T. Dai, C. Wang, Y. Wang, W. Xu, J. Hu and Y. Cheng, *ACS Appl. Mater. Interfaces*, 2018, **10**, 15163–15173.
2 H. Jiang, G. Zhang, F. Li, Y. Zhang, Y. Lei, Y. Xia, X. Jin, X. Feng and H. Li, *Nanoscale*, 2017, **9**, 15470–15476.
3 X. Su and B. Chen, *Carbohydr. Polym.*, 2018, **197**, 497–507.
4 F. Raza, Y. Zhu, L. Chen, X. You, J. Zhang, A. Khan, M. W. Khan, M. Hasnat, H. Zafar, J. Wu and L. Ge, *Biomater. Sci.*, 2019, **7**, 2023–2036.
5 L. Xu, L. Qiu, Y. Sheng, Y. Sun, L. Deng, X. Li, M. Bradley and R. Zhang, *J. Mater. Chem. B*, 2018, **6**, 510–517.
6 H. M. Dao, J. Chen, B. S. Tucker, V. Thomas, H.-W. Jun, X.-C. Li and S. Jo, *ACS Biomater. Sci. Eng.*, 2018, **4**, 2435–2442.
7 S. H. Hong, S. Kim, J. P. Park, M. Shin, K. Kim, J. H. Ryu and H. Lee, *Biomacromolecules*, 2018, **19**, 2053–2061.
8 Y. Zhao, C. Shi, X. Yang, B. Shen, Y. Sun, Y. Chen, X. Xu, H. Sun, K. Yu, B. Yang and Q. Lin, *ACS Nano*, 2016, **10**, 5856–5863.
9 H. J. Sim, T. Thambi and D. S. Lee, *J. Mater. Chem. B*, 2015, **3**, 8892–8901.
10 L. Nebhani, V. Choudhary, H.-J. Adler and D. Kuckling, *Polymers (Basel).*, 2016, **8**, 233.
11 N. Rasool, T. Yasin, J. Y. Y. Heng and Z. Akhter, *Polymer (Guildf).*, 2010, **51**, 1687–1693.
12 K. Pagonis and G. Bokias, *Polym. Bull.*, 2007, **58**, 289–294.
13 E. Mah and R. Ghosh, *Processes*, 2013, **1**, 238–262.
14 J. Park, S. Pramanick, D. Park, J. Yeo, J. Lee, H. Lee and W. J. Kim, *Adv. Mater.*, 2017, **29**, 1702859.
15 X.-H. Qin, X. Wang, M. Rottmar, B. J. Nelson and K. Maniura-Weber, *Adv. Mater.*, 2018, **30**, 1705564.
16 B. Ryplida, K. D. Lee, I. In and S. Y. Park, *Adv. Funct. Mater.*, 2019, 1903209.
17 S. Dutta, P. Samanta and D. Dhara, *Int. J. Biol. Macromol.*, 2016, **87**, 92–100.
18 H. Kono, *Carbohydr. Polym.*, 2014, **106**, 84–93.
19 Abdullah-Al-Nahain, H. Lee, Y. S. Lee, K. D. Lee and S. Y. Park, *Macromol. Biosci.*, 2011, **11**, 1264–1271.
20 R. E. Humphrey and J. L. Potter, *Anal. Chem.*, 1965, **37**, 164–165.
21 J. Krijt, M. Vacková and V. Kozich, *Clin. Chem.*, 2001, **47**, 1821–1828.
22 Y. Wi, H. T. Le, P. Verwilst, K. Sunwoo, S. J. Kim, J. E. Song, H. Y. Yoon, G. Han, J. S. Kim, C. Kang and T. W. Kim, *Chem. Commun.*, 2018, **54**, 8897–8900.
23 F. Inagaki, M. Momose, N. Maruyama, K. Matsuura, T. Matsunaga and C. Mukai, *Org. Biomol. Chem.*, 2018, **16**, 4320–4324.
24 S. Kaur, C. Prasad, B. Balakrishnan and R. Banerjee, *Biomater. Sci.*, 2015, **3**, 955–987.
25 S. A. Elkassih, P. Kos, H. Xiong and D. J. Siegwart, *Biomater. Sci.*, 2019, **7**, 607–617.
26 Y. Su, Y. Hu, Y. Du, X. Huang, J. He, J. You, H. Yuan and F. Hu, *Mol. Pharm.*, 2015, **12**, 1193–1202.
27 N. Sood, A. Bhardwaj, S. Mehta and A. Mehta, *Drug Deliv.*, 2014, 1–23.
28 G. Deen and X. Loh, *Gels*, 2018, **4**, 13.
29 E. B. Kang, J. E. Lee, Z. A. I. Mazrad, I. In, J. H. Jeong and S. Y. Park, *Nanoscale*, 2018, **10**, 2512–2523.
30 S. Li, X. Wang, R. Hu, H. Chen, M. Li, J. Wang, Y. Wang, L. Liu, F. Lv, X.-J. Liang and S. Wang, *Chem. Mater.*, 2016, **28**, 8669–8675.
31 C. A. Choi, J. E. Lee, Z. A. I. Mazrad, Y. K. Kim, I. In, J. H. Jeong and S. Y. Park, *ChemMedChem*, 2018, **13**, 1459–1468.
32 L. Cheng, W. He, H. Gong, C. Wang, Q. Chen, Z. Cheng and Z. Liu, *Adv. Funct. Mater.*, 2013, **23**, 5893–5902.
33 K. Sun, Y. Yang, H. Zhou, S. Yin, W. Qin, J. Yu, D. T. Chiu, Z. Yuan, X. Zhang and C. Wu, *ACS Nano*, 2018, **12**, 5176–5184.
34 Q. Wei, W. Luo, S. Chiang, T. Kappel, C. Mejia, D. Tseng, R. Y. L. Chan, E. Yan, H. Qi, F. Shabbir, H. Ozkan, S. Feng and A. Ozcan, *ACS Nano*, 2014, **8**, 12725–12733.
35 Z. Lin, J. Chen, X. Li, Z. Zhou, K. Meng, W. Wei, J. Yang and Z. L. Wang, *ACS Nano*, 2017, **11**, 8830–8837.
36 Z. A. I. Mazrad, P. T. M. Phuong, C. A. Choi, I. In, K. D. Lee and S. Y. Park, *ChemMedChem*, 2018, **13**, 2437–2447.
37 E. B. Kang, P. T. M. Phuong, G. Lee, S. Lee, I. In and S. Y. Park, *Macromol. Res.*, , DOI:10.1007/s13233-019-7102-8.
38 X. Chen, Z. Yuan, X. Yi, R. Zhuo and F. Li, *Nanotechnology*, 2012, **23**, 415602.
39 X. Peng, F. Song, E. Lu, Y. Wang, W. Zhou, J. Fan and Y. Gao, *J. Am. Chem. Soc.*, 2005, **127**, 4170–4171.
40 G.-Y. Pan, H.-R. Jia, Y.-X. Zhu and F.-G. Wu, *Nanoscale*, 2018, **10**, 2115–2127.
41 E. B. Kang, I. In, K.-D. Lee and S. Y. Park, *J. Ind. Eng. Chem.*, 2017, **55**, 224–233.
42 G. Feng and B. Liu, *Acc. Chem. Res.*, 2018, **51**, 1404–1414.
43 K. Li, Z. Zhu, P. Cai, R. Liu, N. Tomczak, D. Ding, J. Liu, W. Qin, Z. Zhao, Y. Hu, X. Chen, B. Z. Tang and B. Liu, *Chem. Mater.*, 2013, **25**, 4181–4187.
44 H. Yang, Y. Liu, Z. Guo, B. Lei, J. Zhuang, X. Zhang, Z. Liu and C. Hu, *Nat. Commun.*, 2019, **10**, 1789.
45 R. Guo, T. Li and S. Shi, *J. Mater. Chem. C*, 2019, **7**, 5148–5154.
46 Z. A. I. Mazrad, K. Lee, A. Chae, I. In, H. Lee and S. Y. Park, *J. Mater. Chem. B*, 2018, **6**, 1149–1178.
47 C. A. Choi, J. E. Lee, Z. A. I. Mazrad, I. In, J. H. Jeong and S. Y. Park, *J. Ind. Eng. Chem.*, 2018, **63**, 208–219.
48 J. Zheng, H.-T. Liu, B. Wu, C.-A. Di, Y.-L. Guo, T. Wu, G. Yu, Y.-Q. Liu and D.-B. Zhu, *Sci. Rep.*, 2012, **2**, 662.
49 X.-Y. Zhang, Y. Zheng, C.-H. Liu, P.-H. Wang and Y.-Y. Zhu, *RSC Adv.*, 2016, **6**, 55666–55670.
50 E. Bat, E.-W. Lin, S. Saxer and H. D. Maynard, *Macromol. Rapid Commun.*, 2014, **35**, 1260–1265.
51 K. Jain, R. Vedarajan, M. Watanabe, M. Ishikiriyama and N. Matsumi, *Polym. Chem.*, 2015, **6**, 6819–6825.

52 W. J. Zheng, N. An, J. H. Yang, J. Zhou and Y. M. Chen, *ACS Appl. Mater. Interfaces*, 2015, **7**, 1758–1764.

53 A. Ahiabu and M. J. Serpe, *ACS Omega*, 2017, **2**, 1769–1777.

54 X. Liang, L. Fang, X. Li, X. Zhang and F. Wang, *Biomaterials*, 2017, **132**, 72–84.

55 A. GhavamiNejad, M. SamariKhalaj, L. E. Aguilar, C. H. Park and C. S. Kim, *Sci. Rep.*, 2016, **6**, 33594.

56 L. Han, Y. Zhang, X. Lu, K. Wang, Z. Wang and H. Zhang, *ACS Appl. Mater. Interfaces*, 2016, **8**, 29088–29100.

57 J. Hu, Y. Chen, Y. Li, Z. Zhou and Y. Cheng, *Biomaterials*, 2017, **112**, 133–140.

58 C. Ma, Y. Shi, D. A. Pena, L. Peng and G. Yu, *Angew. Chemie Int. Ed.*, 2015, **54**, 7376–7380.

59 Y. Qu, B. Y. Chu, J. R. Peng, J. F. Liao, T. T. Qi, K. Shi, X. N. Zhang, Y. Q. Wei and Z. Y. Qian, *NPG Asia Mater.*, 2015, **7**, e207–e207.

60 F. Zhao, D. Yao, R. Guo, L. Deng, A. Dong and J. Zhang, *Nanomaterials*, 2015, **5**, 2054–2130.

61 A. Paciello and M. G. Santonicola, *RSC Adv.*, 2015, **5**, 88866–88875.

62 M. Karimi, *Smart External Stimulus-Responsive Nanocarriers for Drug and Gene Delivery*, IOP Publishing, 2015.

63 R. E. Rivero, M. A. Molina, C. R. Rivarola and C. A. Barbero, *Sensors Actuators B Chem.*, 2014, **190**, 270–278.

64 Y. Shi, C. Ma, L. Peng and G. Yu, *Adv. Funct. Mater.*, 2015, **25**, 1219–1225.

65 Y. Wei, Q. Zeng, M. Wang, J. Huang, X. Guo and L. Wang, *Biosens. Bioelectron.*, 2019, **131**, 156–162.

66 J. Huang, Q. Zeng, S. Bai and L. Wang, *Anal. Chem.*, 2017, **89**, 8358–8365.

67 M. Qiu, D. Wang, W. Liang, L. Liu, Y. Zhang, X. Chen, D. K. Sang, C. Xing, Z. Li, B. Dong, F. Xing, D. Fan, S. Bao, H. Zhang and Y. Cao, *Proc. Natl. Acad. Sci.*, 2018, **115**, 501–506.

68 F. Yan, W. Duan, Y. Li, H. Wu, Y. Zhou, M. Pan, H. Liu, X. Liu and H. Zheng, *Theranostics*, 2016, **6**, 2337–2351.

View Article Online
DOI: 10.1039/C9BM00734B

View Article Online
DOI: 10.1039/C9BM00734B

Graphical Abstract